Journal of
*Marine Science and Engineering*

MDPI

*Article*

# Experimental and Numerical Investigations for Impact Loading on Platform Decks

**Baolei Geng [1], Keshuai Sun [2,*], Pu Gao [3], Ruijia Jin [1] and Shengchao Jiang [4]**

[1] National Engineering Laboratory for Port Hydraulic Construction, Tianjin Research Institute for Water Transport Engineering, Ministry of Transport of the People's Republic of China, Tianjin 300456, China; gengbaolei@foxmail.com (B.G.)
[2] College of Power and Energy Engineering, Harbin Engineering University, Harbin 264000, China
[3] China State Construction Engineering Corporation Sixth Bureau, Tianjin 300012, China
[4] State Key Laboratory of Coastal and Offshore Engineering, Dalian University of Technology, Dalian 116024, China; jiangshengchao@foxmail.com
* Correspondence: aedc@163.com

**Abstract:** Experimental measurement and numerical simulations were carried out for investigating the impact loading behavior of platform decks under regular and irregular wave actions. In the numerical simulation section, a full-scale numerical wave tank was established using STAR-CCM+ software. A decreased tendency can be observed for an increased relative length of platform when the incident wave length is double the deck length. The increased deck height can also decrease impact loading on the platform, which is due to the platform being far away from the incident wave. Impact loading on the deck decreases with the increase in inclination angle, which can be explained by the deck bottom being directly exposed to the incident wave at negative inclination angles. Finally, the variation tendency of impact loading on platform decks under irregular wave actions is similar to that under regular wave actions, including the averaged values and significant values.

**Keywords:** impact loading; platform deck; wave actions; inclination angles; deck height

check for updates

**Citation:** Geng, B.; Sun, K.; Gao, P.; Jin, R.; Jiang, S. Experimental and Numerical Investigations for Impact Loading on Platform Decks. *J. Mar. Sci. Eng.* **2024**, *12*, 899. https://doi.org/10.3390/jmse12060899

Academic Editors: Shan Wang, Carlos Guedes Soares and Spyros A. Mavrakos

Received: 8 April 2024
Revised: 22 May 2024
Accepted: 24 May 2024
Published: 28 May 2024

**Copyright:** © 2024 by the authors. Licensee MDPI, Basel, Switzerland. This article is an open access article distributed under the terms and conditions of the Creative Commons Attribution (CC BY) license (https://creativecommons.org/licenses/by/4.0/).

## 1. Introduction

The impact of waves is characterized by extremely short durations and complex mechanisms, particularly when changes in structural inclination occur due to uneven settlement of the construction platform, further complicating the study of wave impact issues. Upon contact between wave crests and structures, there exists an intense, short-duration force known as wave impact load. This force can result in localized structural damage or even total overturning, underscoring the significant importance of investigating wave impacts on construction platforms. With the development of offshore resources, traditional construction platforms are no longer sufficient, necessitating the construction of offshore platforms around foundations for construction purposes. These platforms are often directly exposed to wave action, including wave impact, due to the absence of harbors or breakwaters for protection. Research on wave impact issues can be classified into algorithmic studies and model experimentation, based on research methodologies.

Algorithm research comprises theoretical formulation and numerical simulation. Theoretical formulations represent the earliest approach to studying the impact of waves on structures, predominantly focusing on model water entry problems. In 1932, Von Karman [1], based on the principle of momentum conservation, simplified the landing of seaplanes on water surfaces to the process of two-dimensional wedge-shaped structures entering water, analyzing the vertical impact force on the float upon entry and proposing the Von Karman impact theory. The primary drawback of this theory is the infinite impact pressure on the lower plate. Subsequently, Wagner [2], building upon Von Karman's theory of water entry impact, considered the influence of water surface bulging when structures

enter the water and approximated flat plates as small-angle wedge bodies using potential flow theory, deriving an approximate impact theory for flat plates. Studies indicate that this method can be extended to various geometric shapes and non-vertical velocity water entry impact problems, providing estimates of the impact forces on damaged semi-submersible platform pontoons. Riccardi [3], employing the method of conformal mapping, analyzed the early-stage flow generated by the collision of asymmetric wedges. Due to the assumption of inviscid flow, velocity (and pressure) singularities occur at the vertices of asymmetric wedges. By reintroducing viscous effects and shedding vortices from the vertices, these singularities are eliminated. The study analyzed the influence of structure entry into viscous fluids on the free surface and discussed the effects of vortices on the velocity field and pressure distribution on the wedge blocks. Faltinsen [4] and others used potential flow theory to investigate the slamming problem in ship and ocean engineering, demonstrating that the maximum pressure cannot be used to estimate the maximum stress caused by slamming when the maximum pressure is significant. The influence of water elasticity increases with decreasing deadrise angle and increasing impact velocity, emphasizing the need for a fluid dynamics study of slamming from a structural perspective. Sun et al. [5] established a finite element dynamic analysis model of the motion of a three-dimensional elastic projectile in a multi-material fluid medium using the finite element software LS-DYNA, and conducted fluid–structure coupling simulation of the projectile's impact on water using the Arbitrary Lagrangian-Eulerian (ALE) method. Yang et al. [6] performed numerical simulation and analysis of the two-dimensional elastic flat-bottom structure's constant-speed impact into water using the ALE algorithm.

Numerical simulations primarily involve boundary element methods, the VOF method, etc. Xinmeng et al. [7] focused on analyzing higher harmonic load, dynamic motion response, and tension load of the mooring line of the DeepCwind semi-submersible FOWT. The results show that the higher-harmonic wave load cannot be ignored in the extreme marine environment, the second harmonic can be over 16% of the linear wave load, and the third harmonic can be over 10% of the linear wave load with large wave steepness. The duration of a focused wave crest interaction with the platform is a short process of only 1.4 s at the model scale, corresponding to about 10 s for the prototype.

Baarholm et al. [8] conducted numerical simulations of the impact of two-dimensional horizontal plates under regular wave action using the boundary element method, comparing the simulated impact loads with experimental values, which were found to be relatively close. Du Yang et al. [9] studied the impact characteristics of two-dimensional plates entering water using the VOF method, analyzing the relationship between impact loads and entry velocity, transverse velocity, and entry angle. Greenhow and Moyo [10] identified the influence of rising free surface and added mass on both local and overall structures. Chen et al. [11] conducted numerical simulations of the two-dimensional wedge entry slamming problem using the Smoothed Particle Hydrodynamics (SPH) method, analyzing the variations in structure entry speed and slamming load. They derived the relationship between the entry angle, speed of the wedge, and slamming pressure. Wang et al. [12] employed dynamic mesh technology and the Volume of Fluid (VOF) method to simulate the free entry process of flat-bottom structures and two-phase gas–liquid flow. They analyzed the motion characteristics of the structure during free fall, the characteristics of slamming loads, and the evolution of air bubbles during entry into water. Du et al. [13] sloshing coupled ship motions are solved numerically in a time domain approach, in which the external flow and sloshing are computed respectively with linear diffraction-radiation theory and the Arbitrary Lagrangian-Eulerian method. In this numerical method, the structure flexibility of the tank wall could be included without additional computational effort.

Due to the complexity of the phenomena and mechanisms involved in wave impact, the study of wave impact in marine environments can be approached through physical model experiments. Nagi et al. [14] conducted model tests to investigate the global response of a conventional tension leg platform (TLP) due to wave-in-deck loads associated with extreme wave events in irregular long-crested waves of a cyclonic sea state. The experi-

mental setup was designed to allow for the simultaneous measurement of wave surface elevations, rigid body motions, tendon tensions, as well as the pressure distribution at the model's deck underside. Min et al. [15,16] conducted an experimental campaign focusing on two air-gap conditions (i.e., 0.35 Hc and 0.2 Hc, where Hc is the height of the platform column) and various wave impact patterns. Multiple quantities have been measured for each experimental test, including platform motions, tension forces in tethers, and the wave impact pressure at numerous locations within the structure. Within the experimental cases tested, it is found that (i) with the reduction in the air gap, the impact pressure at the bottom wall of the upper deck increases while that at the vertical front wall reduces; (ii) the air gap of 0.55 Hc registers larger surge motions as compared to other air-gap conditions due to the combined effect of larger horizontal loads applied on the platform and the small resistance force of the system.

Cuomo et al. [17] conducted physical model experiments to study the slamming effects of wave breaking on offshore bridges. They elucidated the slamming response process between waves and structures, proposing an "ad-hoc" predictive method for pulse pressure and quasi-static pressure tailored for large-scale structures. Ren and Wang [18], employing physical model experimental methods, investigated the impact on the upper part of perforated structures under irregular wave action. They discussed the influence of various wave parameters and structural porosity on the peak impact pressure and provided the distribution characteristics of the peak impact pressure on the structure's bottom surface. Zhou et al. [19] conducted a series of model experiments to study the uplift force acting on perforated plates under regular wave action. They analyzed the mechanism of the wave uplift force on the bottom of the plate and discussed the relationship between the maximum uplift force and wave parameters, impact angles, and the air cushion layer, providing a formula for calculating the maximum total uplift force on perforated horizontal plates under waves. Paulsen et al. [20] investigated the slamming effects of wind and waves on offshore wind turbine pile foundations through physical model experiments. They analyzed the wave impact effects on pile foundations under irregular wave action, revealing a higher frequency of wave slamming in the transition zone near the free surface.

In summary, theoretical analyses are mostly based on various ideal assumptions that do not align with actual fluid behavior. Model experiments are often conducted using scaled-down models, but despite significant effort, it is challenging to achieve complete similarity between the model and the real structure, and many detailed issues cannot be thoroughly investigated. Therefore, we employ a combined approach of algorithms and experiments to explore the impact of waves on platforms. Most numerical simulations focus on the slamming problems of two-dimensional structures and predominantly consider regular waves without incorporating irregular wave analysis. This study establishes and validates a three-dimensional numerical model of a platform and water tank using CFD software to investigate the slamming effects of waves on a deep-water rigid platform under both regular and irregular wave conditions. For each wave type, the influence of platform inclination and height, as well as the incident wave height and period on slamming pressure, is discussed. The present study summarizes the effects of different platform inclinations and heights, various wave heights, and different relative plate lengths on the slamming behavior of the rigid platform.

In Section 2, the experimental setup and numerical wave flume is introduced. In Section 3, numerical validations of the numerical model against experimental data are conducted. The experimental and numerical results and discussions are presented in Sections 4 and 5, where the behavior of impact loading under regular and irregular wave actions is investigated, respectively. Finally, conclusions are drawn in Section 6.

## 2. Experimental Setup and Numerical Models

### 2.1. Experimental Setup

The experiments are conducted in a three-dimensional wave basin at Ho-Hai University, China. The wave basin is 42 m long and 12 m wide, and the water depth is 0.6 m in

the tests. Regular and irregular waves are generated by paddles. The wave absorbers are installed on the opposite side to minimize reflected waves. In the experiment, the scope of regular wave height is $H_i$ = 0.04–0.08 m, with wave periods varying from 0.85 s to 1.98 s. The length scaling with Froude similarity is 1:50.

The platform is located in the center of the wave basin, which is made of wood and trusses. The platform deck is 1.0 m in length and 1.0 m wide, with a 0.1 m thickness. Five deck angles, that is, $\alpha = -4°$, $-2°$, $0°$, $2°$, and $4°$, are selected, as shown in Figure 1. In total, 32 probes are adopted for measuring the impact pressure of the platform deck, where the sampling frequency is 50 Hz. The distribution of pressure probes is shown in Figure 2.

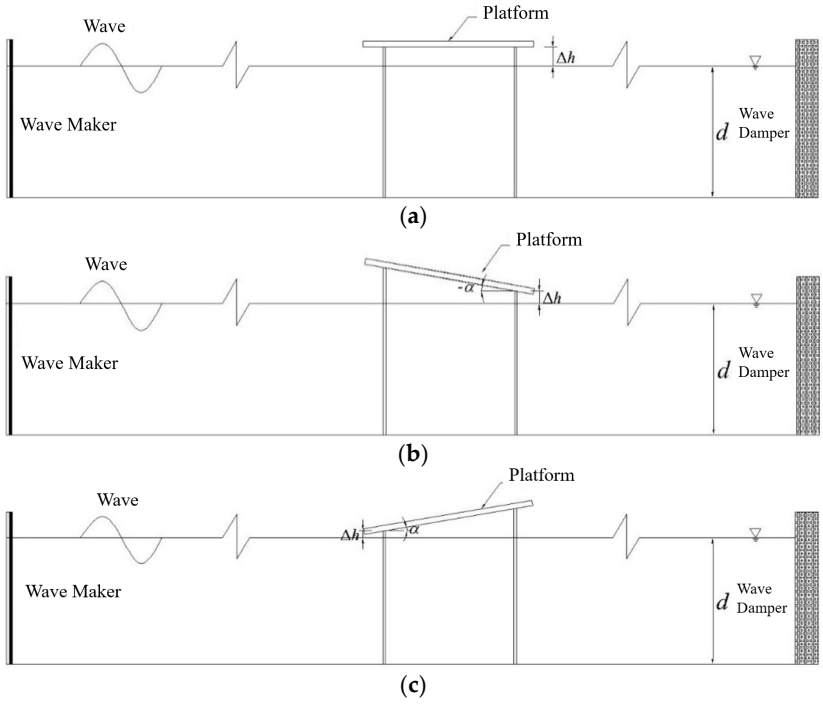



**Figure 1.** Snapshots of model ship in waves and sloshing motion in tank. (**a**) Horizontal platform ($\alpha = 0°$). (**b**) Inclination $\alpha$ is less than zero ($\alpha < 0°$). (**c**) Inclination $\alpha$ is greater than zero ($\alpha > 0°$).

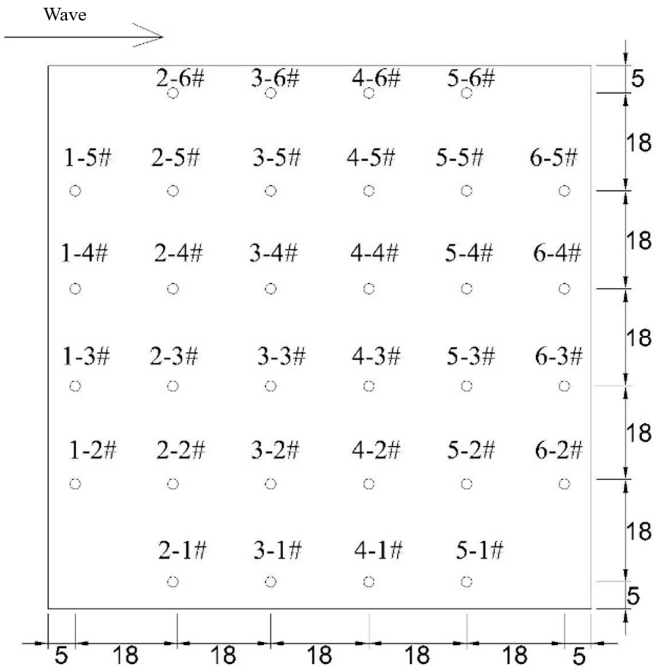



**Figure 2.** Sketch of pressure transducers on subsurface (unit: cm).

*2.2. Numerical Approaches*

The numerical wave flume is conducted by solving the Navier-Stokes equations; incompressible two-phase turbulent flows with the RNG model is used in the simulation and the Eulerian reference system is adopted. Thus, the governing equations are written as follows:

$$\begin{array}{l} \frac{\partial \rho u_i}{\partial x_i} = 0 \\ \frac{\partial \rho u_i}{\partial t} + \frac{\partial \rho u_j u_i}{\partial x_j} = \rho g_i - \frac{\partial p}{\partial x_i} + \mu_e \frac{\partial}{\partial x_j}\left(\frac{\partial u_i}{\partial x_j} + \frac{\partial u_j}{x_i}\right) \end{array} \quad (1)$$

where $u_i = (u, v)$ and $x_i = (x, y)$ are the vector of fluid velocity and the Cartesian coordinate, respectively. $g_i$ denotes the gravitational acceleration; $\rho$ denotes the fluid density; $p$ denotes the pressure; and t denotes the time. In the equation, $\mu_e$ presents the effective dynamic viscosity and is composed of $\mu$ and $\mu_t$, $\mu$ is the fluid viscosity, and $\mu_t$ is the turbulent viscosity. For closing the governing equations, the RNG $k$-$\varepsilon$ two-equation formulations are employed, with

$$\mu_t = C_\mu \frac{k^2}{\varepsilon} \quad (2)$$

where $C_\mu = 0.0845$. The time-dependent advection-diffusion equations for the turbulent kinematic energy $k$ and its dissipation rate $\varepsilon$ are described as follows:

$$\frac{\partial \rho k}{\partial t} + \frac{\partial}{\partial x_j}\left[\rho u_j k\right] = \frac{\partial}{\partial x_j}\left(\frac{\mu_t}{\sigma_k}\frac{\partial k}{\partial x_j}\right) + \mu_t\left(\frac{\partial u_i}{\partial x_j} + \frac{\partial u_j}{\partial x_i}\right)\frac{\partial u_i}{\partial x_j} - \rho\varepsilon \quad (3)$$

$$\frac{\partial \rho \varepsilon}{\partial t} + \frac{\partial}{\partial x_j}\left[\rho u_j \varepsilon\right] = \frac{\partial}{\partial x_j}\left(\frac{\mu_t}{\sigma_\varepsilon}\frac{\partial \varepsilon}{\partial x_j}\right) + C_{1\varepsilon}\frac{\varepsilon}{k}\mu_t\left(\frac{\partial u_i}{\partial x_j} + \frac{\partial u_j}{\partial x_i}\right)\frac{\partial u_i}{\partial x_j} - \rho C_{2\varepsilon}\frac{\varepsilon^2}{k} \quad (4)$$

where $C_{1\varepsilon} = 1.42$, $C_{2\varepsilon} = 1.68$, $\sigma_k = 0.71942$, and $\sigma_e = 0.71942$, which are theoretical constants.

For long-time simulations in the present numerical wave flume, reflection waves should be eliminated. The toolbox "waves2Foam" proposed by Jacobsen et al. [21] is utilized; relaxation zones are placed at both inlet and outlet boundaries to generate the incident waves and eliminate reflected waves. The exponential relaxation function is applied within the relaxation zones as follows:

$$\varphi_R(\chi_R) = 1 - \frac{\exp\left(\chi_R^{3.5}\right) - 1}{\exp(1) - 1}, \ \chi_{R\in[0,1]} \quad (5)$$

$$\vartheta = \varphi_R \vartheta_C + (1 - \varphi_R)\vartheta_T \quad (6)$$

where $\vartheta$ represents both the fluid velocity $u_i$ and the water fraction indicator $\alpha$, the subscript $C$ denotes the computed value, and the subscript $T$ denotes the target value.

To capture the free surface motion in the present wave flume, the volume of fluid (VOF) method is used. For computational cells, a fractional function of the VOF, denoted as $\phi$, is defined as

$$\begin{cases} \phi = 0 \text{ inair} \\ 0 < \phi < 1 \text{ on the free surface} \\ \phi = 1 \text{ in water} \end{cases} \quad (7)$$

The VOF function is governed by the advection equation:

$$\frac{\partial \phi}{\partial t} + \nabla \cdot (\phi \mathbf{u}) + \nabla \cdot [\phi(1 - \phi)\mathbf{u}_r] = 0 \quad (8)$$

where $\mathbf{u}_r$ is the relative velocity between the water and air. In Equation (8), the last term of the left hand is for compression, which is used to limit the smearing of the interface. In the present work, the interface of the two different phases is identified when $\phi = 0.5$. In the

computational cells, the fluid density and the effective viscosity are weighed by using the VOF function as follows:

$$\begin{aligned} \rho &= \phi\rho_W + (1-\phi)\rho_A \\ \mu_e &= \phi\mu_{eW} + (1-\phi)\mu_{eA} \end{aligned} \tag{9}$$

where the subscript $W$ represents the water phase and $A$ is the air phase.

The governing equations and the advection transport equation are solved by using the Finite Volume Method (FVM) based on the multi-phase solver of "interFoam" in OpenFOAM® package. The pressure and velocity decoupling is solved by using the PISO (Pressure Implicit with Splitting of Operators) algorithm (Issa [22]). The convection term and diffusion term are discretized by the Gauss limited linear method and the Gauss linear corrected method, respectively.

Courant–Friedrichs–Lewy (CFL) condition is adopted in all of the numerical simulation solving processes, the largest Courant number is set as $C_r$ = 0.25, and the time step adjusts automatically:

$$\Delta t = C_r \times \mathrm{Min}\left\{\frac{\sqrt{S_e}}{|u_e|}\right\} \tag{10}$$

where $S_e$ and $|u_e|$ are the area and absolute velocity in a computational cell, respectively.

## 3. Numerical Validation

Numerical validations are carried out according to the comparison with the experimental data of regular wave actions, with $T$ = 1.70 s and $H$ = 0.08 m, where a platform deck height above the still water level $\Delta h$ = 0 m and inclination angles $\alpha = -4°$, $-2°$, and $0°$ are considered. As shown in Figure 3, good agreement between the numerical results and experimental results can be observed, implying that the present numerical model can work well in predicting impact loading under regular wave actions.

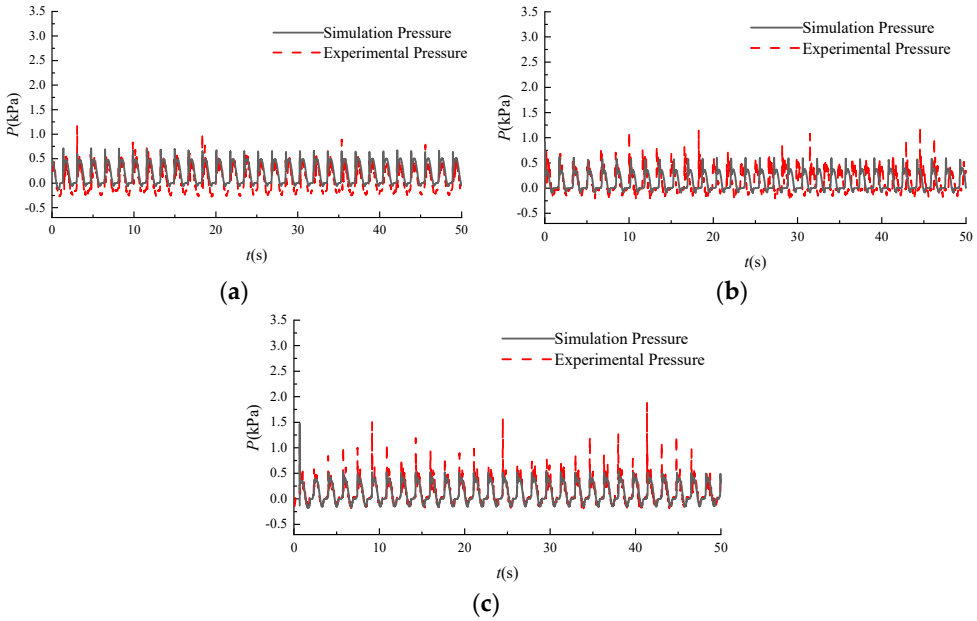



**Figure 3.** Comparison of slamming pressure time history curves at 2–4# measuring points of platforms with different inclination angles under regular wave action. (**a**) $\alpha = -4°$. (**b**) $\alpha = -2°$. (**c**) $\alpha = 0°$.

As shown in Figure 4, further validations are conducted by the comparison of irregular wave actions, where the incident wave conditions are $T_p$ = 1.70 s and $H_s$ = 0.08 m. The geometry of the platform deck is still $\Delta h$ = 0 m with inclination angles $\alpha = -4°$, $-2°$, and $0°$. Compared with the accuracy of regular wave actions in Figure 3, the discrepancy between the numerical and experimental results is a little increased. This is mainly due to the random characteristics of irregular waves. Generally speaking, acceptable accuracy can be

obtained by using the present viscous fluid flow model. According to the comparisons, it can be confirmed that the present numerical wave flume can work well in predicting the behavior of impact loading on the platform deck under regular and irregular wave actions.

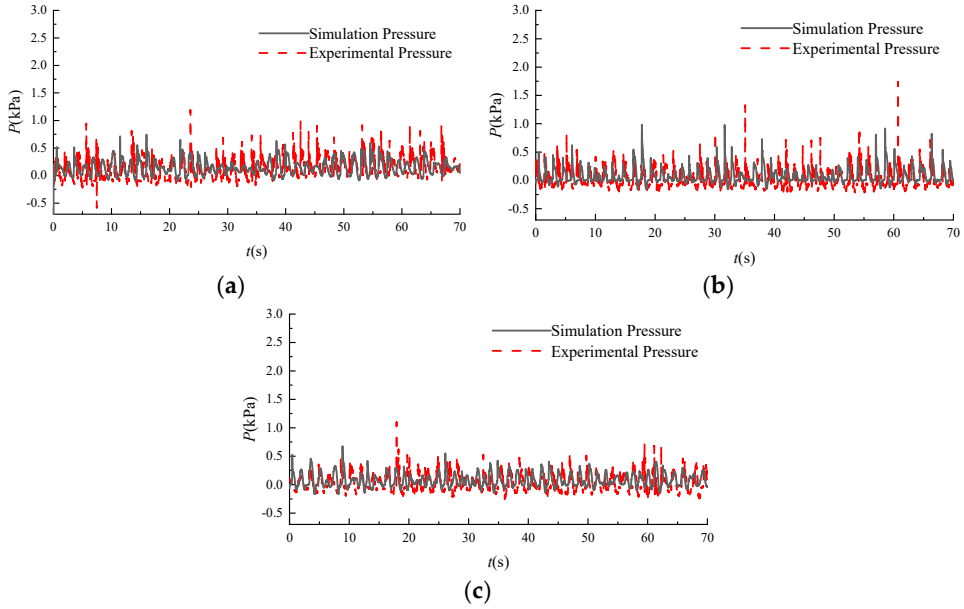



**Figure 4.** Comparison of slamming pressure time history curves at 2–4# measuring points of platforms with different inclination angles under irregular wave action. (**a**) $\alpha = -4°$. (**b**) $\alpha = -2°$. (**c**) $\alpha = 0°$.

## 4. Impact Loading of Regular Waves

Both laboratory tests and numerical simulations are carried out for measuring impact loading on the platform deck under regular waves. Note that the impact forces of the experimental measurement are obtained by the pressure probes multiplied by the corresponding area; meanwhile, the impact forces of the numerical model are calculated according to the integral and the body surface. This is also the major reason for the discrepancy between the experimental and numerical results. Figure 5 shows the variation in the impact loading forces with the relative length of platform $L_B/L$, where $L_B$ and $L$ are the platform length and wave length, respectively. Again, good agreement between the experimental and numerical results can be observed, implying acceptable accuracy of the present simulating method. When the relative length of the platform $L_B/L$ is larger than 0.4, the impact loading forces show a decreased tendency with the relative platform length $L_B/L$. It can be understood that the long wave has more energy and generates increased impact loading on a small relative platform length $L_B/L$. In the region of $L_B/L$ = 0.2–0.4, the variation in the impact loading forces has different behavior patterns at different inclination angles $\alpha$, different heights of the platform deck $\Delta h$, and different incident wave heights $H_i$.

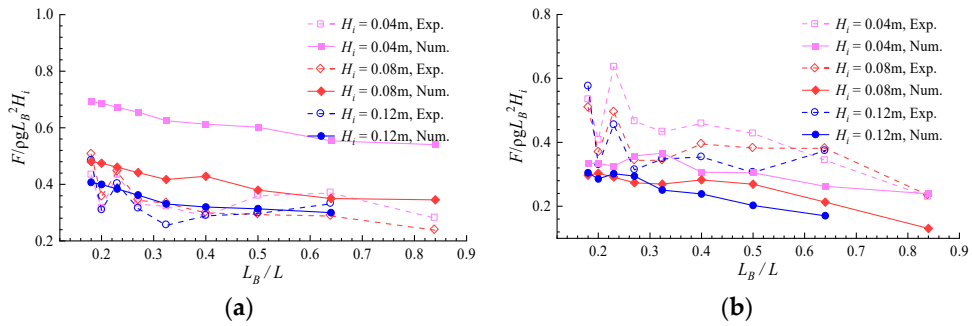



**Figure 5.** *Cont.*

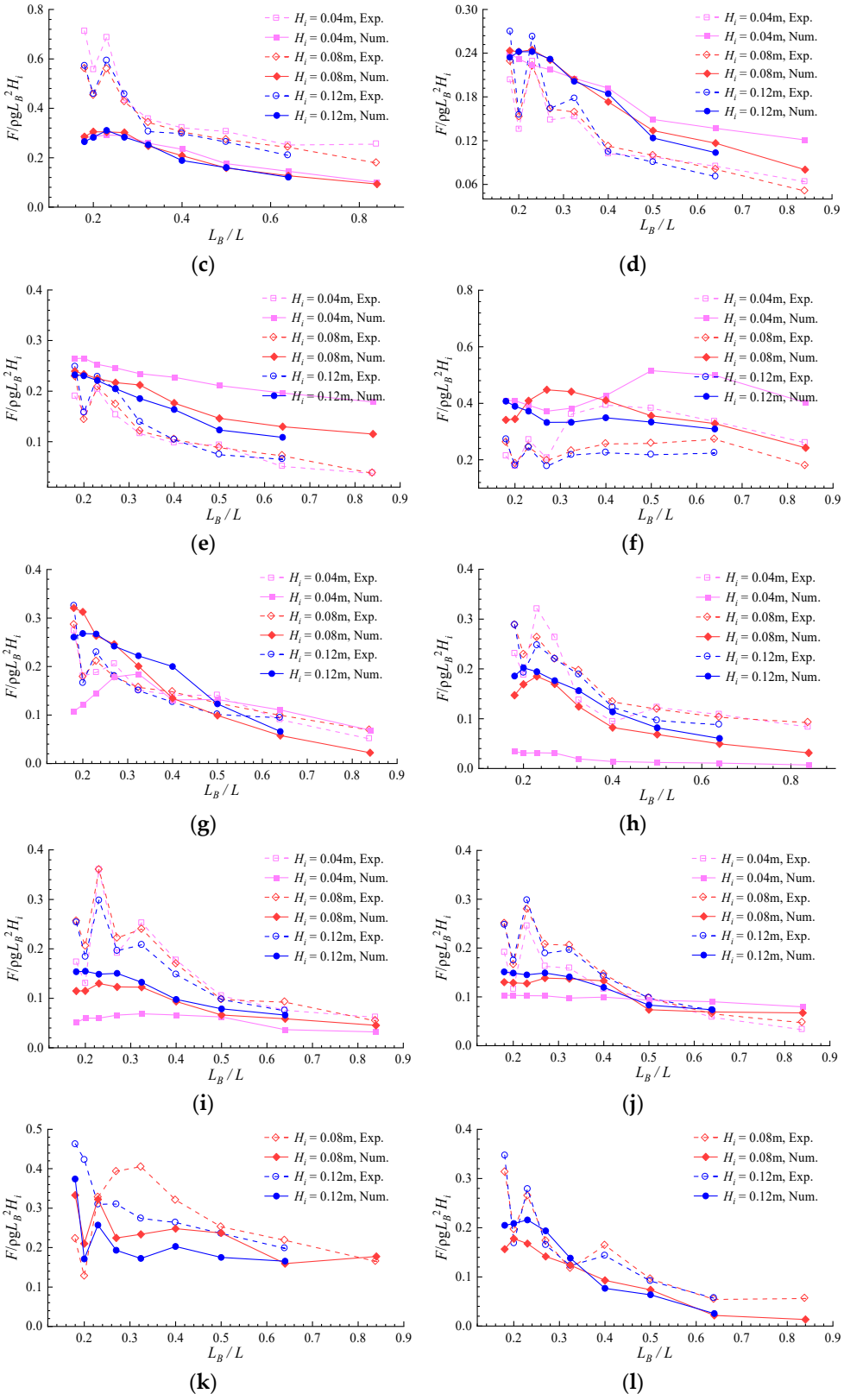



**Figure 5.** *Cont.*

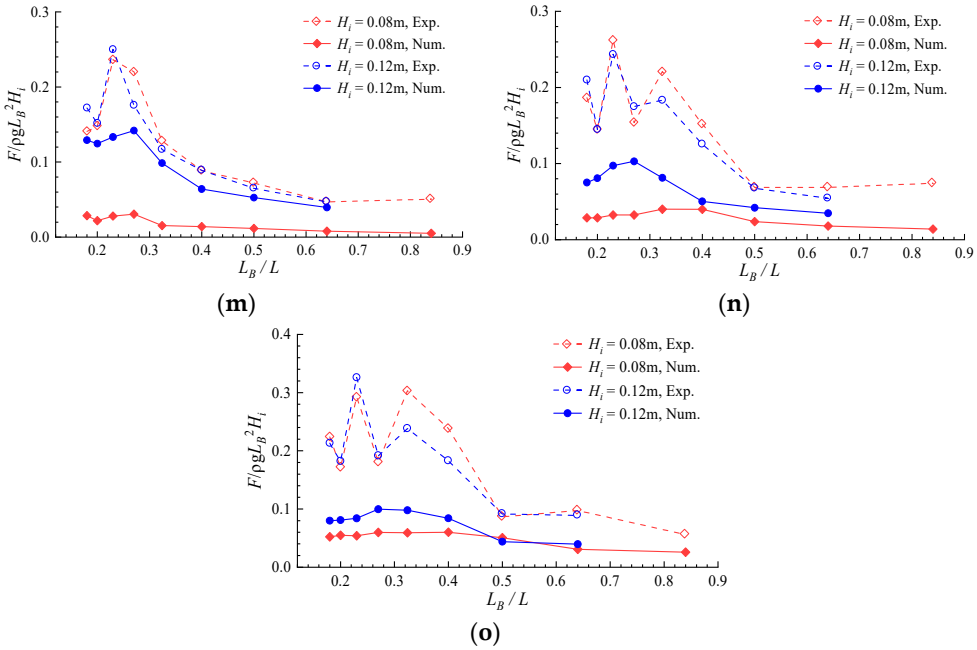



**Figure 5.** Relationship between slamming pressure force and relative wavelength of platforms with different inclination angles under action of regular waves. (**a**) $\alpha = -4°$; $\Delta h = 0$ m. (**b**) $\alpha = -2°$; $\Delta h = 0$ m. (**c**) $\alpha = 0°$; $\Delta h = 0$ m. (**d**) $\alpha = 2°$; $\Delta h = 0$ m. (**e**) $\alpha = 4°$; $\Delta h = 0$ m. (**f**) $\alpha = -4°$; $\Delta h = 0.02$ m. (**g**) $\alpha = -2°$; $\Delta h = 0.02$ m. (**h**) $\alpha = 0°$; $\Delta h = 0.02$ m. (**i**) $\alpha = 2°$; $\Delta h = 0.02$ m. (**j**) $\alpha = 4°$; $\Delta h = 0.02$ m. (**k**) $\alpha = -4°$; $\Delta h = 0.04$ m. (**l**) $\alpha = -2°$; $\Delta h = 0.04$ m. (**m**) $\alpha = 0°$; $\Delta h = 0.04$ m. (**n**) $\alpha = 2°$; $\Delta h = 0.04$ m. (**o**) $\alpha = 4°$; $\Delta h = 0.04$ m.

The influence of the geometries of the platform deck, that is, inclination angles $\alpha$ and the height $\Delta h$, can also be observed according to the comparison between the subfigures in Figure 5. The impact loading on the deck decreases with the increase in inclination angle, that is, the $\alpha$ range from $-4°$ to $4°$. It can be explained that the deck bottom is directly exposed to the incident wave when the inclination angle is $\alpha = -4°$; meanwhile, it is the opposite case when the inclination angle is $\alpha = 4°$. The increased deck height, that is, following the sequence of $\Delta h = 0$, 0.02 and 0.04 m, can also decrease the impact loading on the platform. The increased deck height is able to make the platform far away from the incident wave, leading to the decrease in impact loading.

For the purpose of comparison, the influence of incident wave height on impact loading is also considered. As shown in Figure 5c, the insignificant effect of incident wave height on the normalized impact loading force can be observed for the case of an inclination angle $\alpha = 0°$ and a deck height $\Delta h = 0$ m. In Figure 5h, the impact force of an incident wave height $H_i = 0.04$ m approaches zero, which is due to the fact that small wave heights cannot reach the platform deck with $\Delta h = 0.02$ m. Meanwhile, the normalized impact loading forces have a small increase for incident wave heights from $H_i = 0.08$ m to 0.12 m. When the platform deck height is $\Delta h = 0.04$ m, only the case with $H_i = 0.12$ m has an impact loading force, as shown in Figure 5m. The above phenomena are also suitable for the cases in Figure 5d,g–j,l–o. That is, the variation in Figure 5a,b,e,f,k has different behavior patterns, where the decreased normalized impact loading forces in relation to the increases in wave height can be observed. This demonstrates the complex influence of large inclination angles, $\alpha = -4°$ and $4°$, at which part of the platform deck is submerged in water.

## 5. Impact Loading of Irregular Waves

The behavior of impact loading on the platform deck under irregular wave actions is considered in this section. The region of significant wave heights of irregular waves is $H_s = 0.04$–$0.08$ m, and the peak frequency of the JONSWAP spectrum is 0.85 s–2.26 s. Figure 6 shows the variation in impact loading with the relative length of the platform $L_B/L_s$, where $L_s$ is the

corresponding wave length of significant wave heights of irregular waves. The results of the impact loading forces in the figure are also the significant wave height values. For the purpose of comparison, the numerical results under regular wave actions are also included. It can be observed that the general variation tendency under irregular wave actions is similar with that under regular wave actions. That is, the impact loading forces decrease when the relative length of the platform $L_B/L_s$ is larger than 0.4. The variations in the region of $L_B/L_s$ = 0.2–0.4 have different behavior patterns at different inclination angles $\alpha$, different heights of the platform deck $\Delta h$, and different incident wave heights $H_s$. The increased impact loading force with the decrease in inclination angle and decrease in deck height can be obtained. Finally, the values between regular wave actions and irregular wave actions in Figure 6 are in fact quite close to each other.

Furthermore, the results of the impact loading forces under irregular wave actions between different statistical samplings are compared in Figure 7. Note that the normalized amplitudes are illustrated in this figures, where the normalization is conducted by using the corresponding statistical data, such as $F_s/\rho g L_B{}^2 H_s$ and $F_{ave}/\rho g L_B{}^2 H_{ave}$. In Figure 7a–f, the normalized amplitudes of the impact loading forces computed from the samples with large amplitudes are always smaller than those of the samples with small amplitudes. That is, the values of $F_s/\rho g L_B{}^2 H_s$ are smaller than $F_{ave}/\rho g L_B{}^2 H_{ave}$. It can be understood that larger wave amplitudes may generate more dissipation when the platform deck is submerged in water. In contrast, as shown in Figure 7g–o, the normalized amplitudes of the impact loading forces computed from the samples with large amplitudes are always larger than those of the samples with small amplitudes. This is due to the increased nonlinear effect of impact behavior when the platform deck is above the still water level.

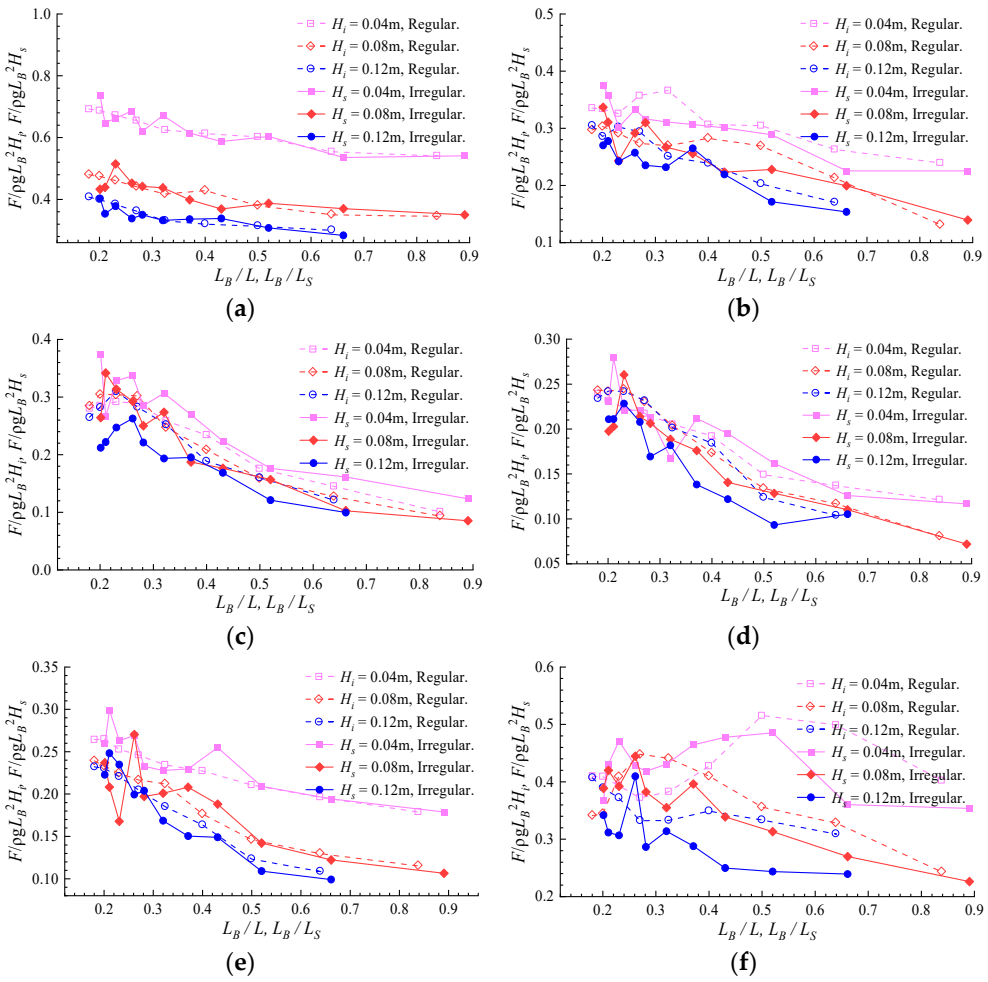



**Figure 6.** *Cont.*

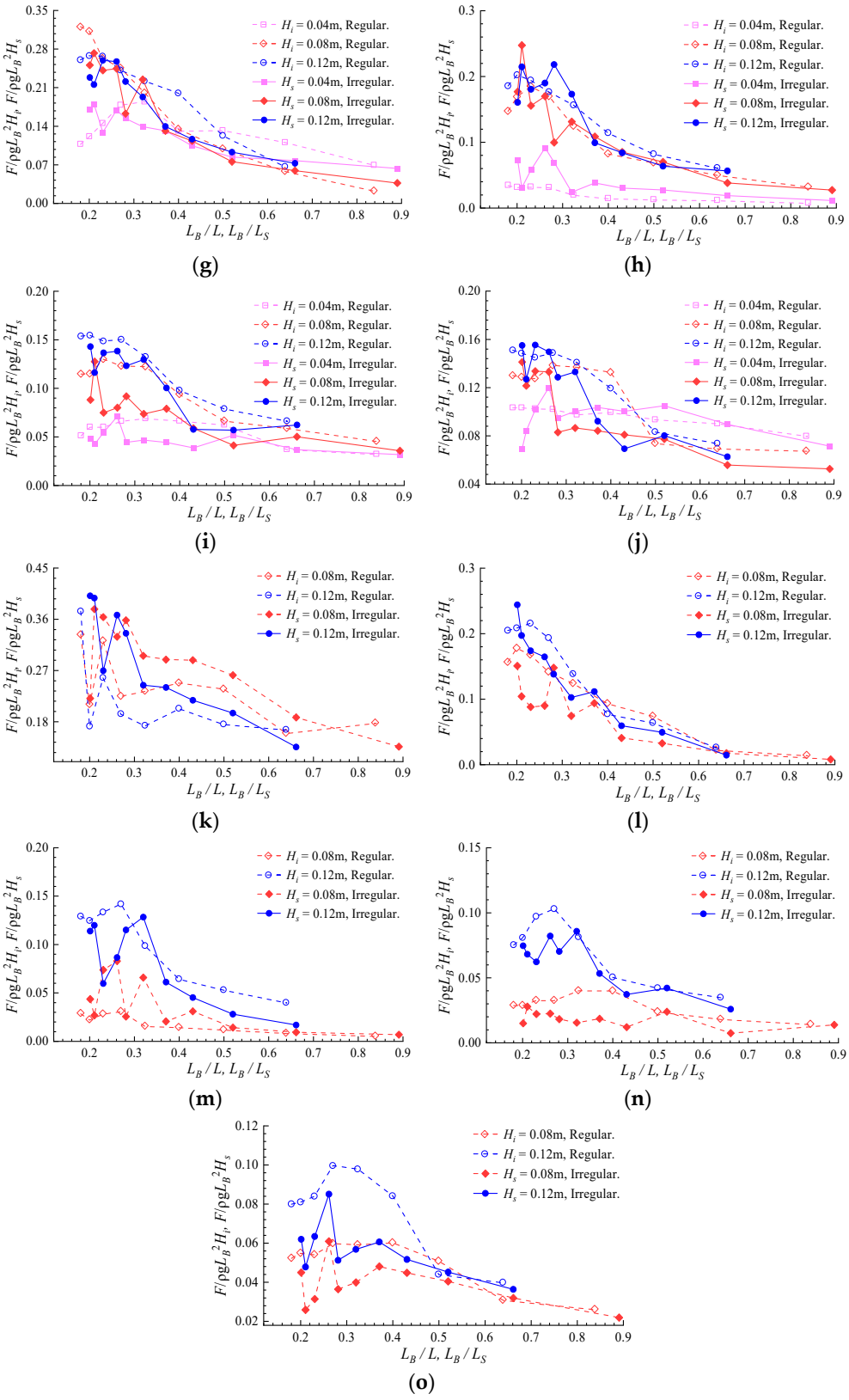



**Figure 6.** Relationship between slamming pressure force and relative wavelength of platforms with different inclination angles under action of irregular waves. (**a**) $\alpha = -4°$; $\Delta h = 0$ m. (**b**) $\alpha = -2°$; $\Delta h = 0$ m. (**c**) $\alpha = 0°$; $\Delta h = 0$ m. (**d**) $\alpha = 2°$; $\Delta h = 0$ m. (**e**) $\alpha = 4°$; $\Delta h = 0$ m. (**f**) $\alpha = -4°$; $\Delta h = 0.02$ m. (**g**) $\alpha = -2°$; $\Delta h = 0.02$ m. (**h**) $\alpha = 0°$; $\Delta h = 0.02$ m. (**i**) $\alpha = 2°$; $\Delta h = 0.02$ m. (**j**) $\alpha = 4°$; $\Delta h = 0.02$ m. (**k**) $\alpha = -4°$; $\Delta h = 0.04$ m. (**l**) $\alpha = -2°$; $\Delta h = 0.04$ m. (**m**) $\alpha = 0°$; $\Delta h = 0.04$ m. (**n**) $\alpha = 2°$; $\Delta h = 0.04$ m. (**o**) $\alpha = 4°$; $\Delta h = 0.04$ m.

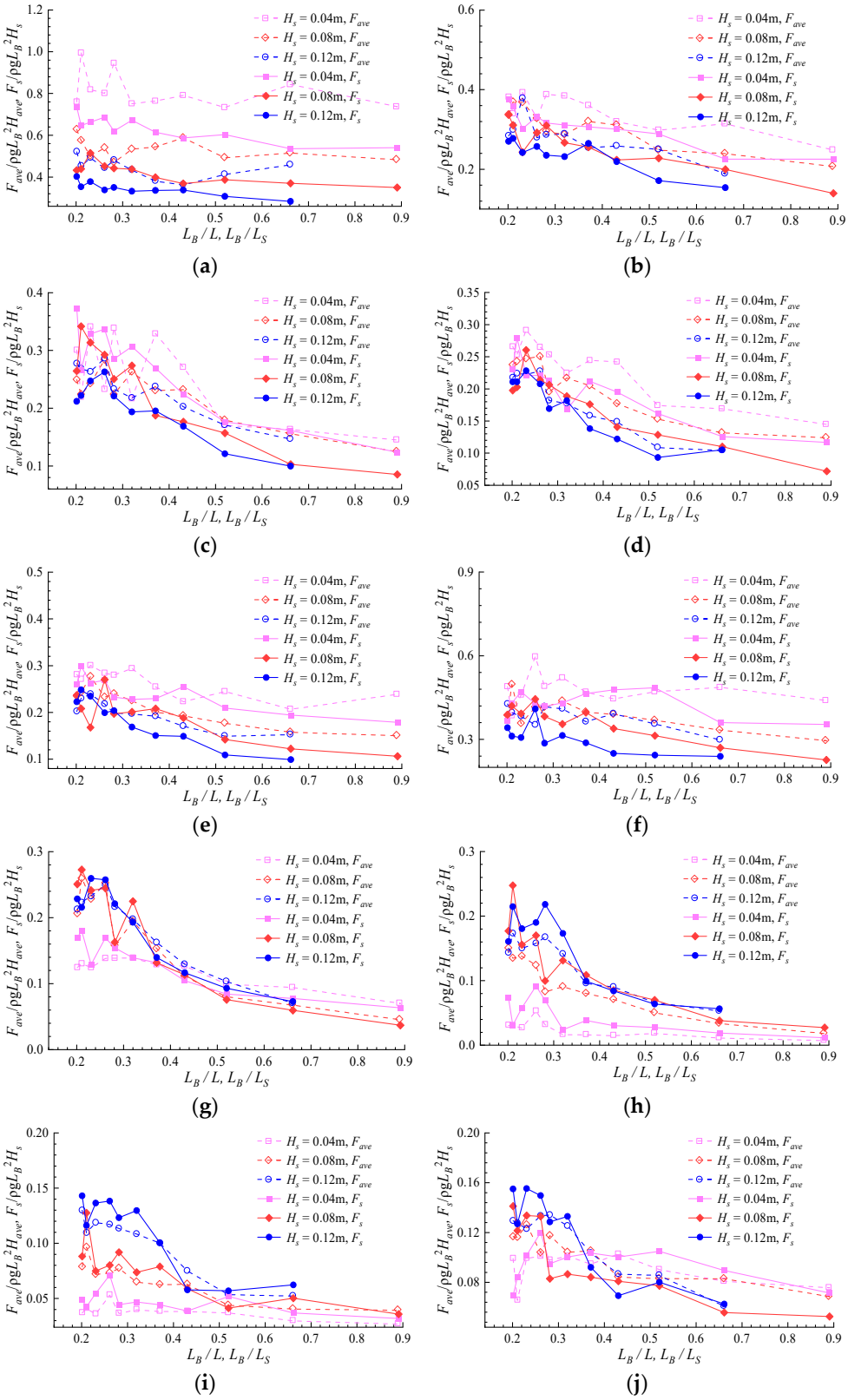



**Figure 7.** *Cont.*

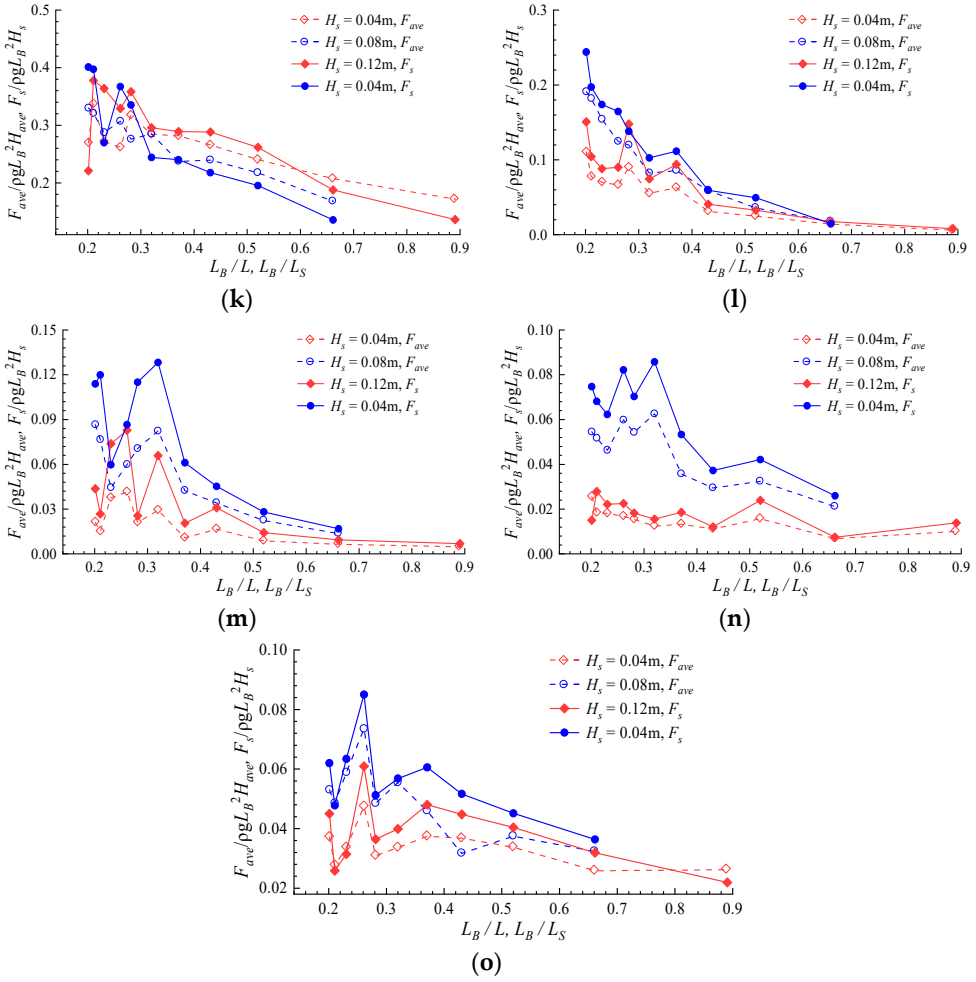



**Figure 7.** Relationship between slamming pressure force and relative wavelength of platforms with different inclination angles under action of irregular waves. (**a**) $\alpha = -4°$; $\Delta h = 0$ m. (**b**) $\alpha = -2°$; $\Delta h = 0$ m. (**c**) $\alpha = 0°$; $\Delta h = 0$ m. (**d**) $\alpha = 2°$; $\Delta h = 0$ m. (**e**) $\alpha = 4°$; $\Delta h = 0$ m. (**f**) $\alpha = -4°$; $\Delta h = 0.02$ m. (**g**) $\alpha = -2°$; $\Delta h = 0.02$ m. (**h**) $\alpha = 0°$; $\Delta h = 0.02$ m. (**i**) $\alpha = 2°$; $\Delta h = 0.02$ m. (**j**) $\alpha = 4°$; $\Delta h = 0.02$ m. (**k**) $\alpha = -4°$; $\Delta h = 0.04$ m. (**l**) $\alpha = -2°$; $\Delta h = 0.04$ m. (**m**) $\alpha = 0°$; $\Delta h = 0.04$ m. (**n**) $\alpha = 2°$; $\Delta h = 0.04$ m. (**o**) $\alpha = 4°$; $\Delta h = 0.04$ m.

## 6. Conclusions

Experimental and numerical simulations have been carried out for impact loading behavior on platform decks under regular and irregular wave actions. The behavior of impact loading forces has different characteristics for different relative lengths of the platform deck. A decreased tendency can be observed when the relative length of the platform $L_B/L$ is larger than 0.4. In the region of $L_B/L$ = 0.2–0.4, the variation in the impact loading forces has different behavior patterns at different inclination angles, different heights of the platform deck, and different incident wave heights. The impact loading on the deck decreases with the increase in inclination angle, which can be explained by the fact that the deck bottom is directly exposed to the incident wave at negative inclination angles. The increased deck height can also decrease impact loading on the platform, which is due to the platform being far away from the incident wave. Finally, the variation tendency of impact loading on the platform deck under irregular wave actions is similar to that under regular wave actions, including the averaged values and significant values.

To simplify the slamming problem, we assumed the offshore platform to be rigid. In reality, the platform would deform under wave-induced slamming forces. Therefore, further research is needed to address the issue of structural deformation under complex wave conditions. The numerical wave tank simulation was conducted with a flat seabed and

a fixed water depth, whereas actual marine environments are more complex, with uneven seabeds and submerged reefs that can cause unpredictable changes in wave height and wavelength. The impact of slamming forces on the platform varies under different wave conditions, necessitating additional research to understand these effects comprehensively.

**Author Contributions:** Conceptualization, B.G., S.J., P.G. and K.S.; methodology, B.G., S.J., P.G. and K.S.; software, P.G., R.J. and S.J.; validation, B.G., P.G. and R.J.; formal analysis, B.G., P.G. and K.S.; investigation, P.G., S.J. and R.J.; resources, B.G., P.G. and R.J.; data curation, B.G., K.S. and S.J.; writing—original draft preparation, B.G., S.J. and K.S.; writing—review and editing, B.G., S.J. and K.S.; visualization, B.G. and S.J.; supervision, K.S. and S.J.; project administration, K.S. and S.J.; funding acquisition, K.S. and S.J. All authors have read and agreed to the published version of the manuscript.

**Funding:** This study is supported by the National Natural Science Foundation of China (U2106223), the Science and Technology Research and Development Project of CSCES (CSCEC-2020-Z-21), and the Basic Funding of the Central Public Research Institutes (TKS20230106).

**Data Availability Statement:** Data will be made available on request.

**Acknowledgments:** All authors have read and agreed to the published version of the manuscript.

**Conflicts of Interest:** The authors declare no conflicts of interest.

## References

1. Von Karman, T. *The Impact of Seaplane Floats during Landing*; National Advisory Committee for Aeronautics: Washington, DC, USA, 1929.
2. Wagner, H. *Landing of Seaplanes*; National Advisory Committee for Aeronautics: Washington, DC, USA, 1931.
3. Riccardi, G.; Iafrati, A. Water impact of an asymmetric floating wedge. *J. Eng. Math.* **2004**, *49*, 19–39. [CrossRef]
4. Faltinsen, O.M. Hydroelastic slamming. *J. Mar. Sci. Technol.* **2000**, *5*, 49–65. [CrossRef]
5. Sun, Q.; Zhou, J.; Lin, P. Dynamic analysis of fluidstructure interaction for water impact of projectile using LS-DYN. *J. Syst. Simul.* **2010**, *22*, 1498–1501.
6. Yang, L.; Zhou, Y.; Li, H.; Wang, K.; Zhang, Y. Research on impact characteristics of water entry of a flat-bottom structure based on ALE method. *Ship Sci. Technol.* **2017**, *39*, 125–133.
7. Zeng, X.; Shi, W.; Feng, X.; Shao, Y.; Li, X. Investigation of higher-harmonic wave loads and low-frequency resonance response of floating offshore wind turbine under extreme wave groups. *Mar. Struct.* **2023**, *89*, 103401. [CrossRef]
8. Baarholm, R.; Faltinsen, O.M. Wave impact underneath horizontal decks. *J. Mar. Sci. Technol.* **2004**, *9*, 1–13. [CrossRef]
9. Du, Y.; Jiang, C.; Zheng, M. VOF Model-Based Study on Slamming Load of Flat-Bottom Structure during Constant-Velocity Water Entry. *China Pet. Mach.* **2020**, *48*, 72–79.
10. Greenhow, M.; Moyo, S. Water Entry and Exit of a Horizontal Circular Cylinder. *Appl. Ocean. Res.* **2005**, *10*, 191–198. [CrossRef]
11. Chen, G.; Zheng, X.; Wu, X.; Zhang, H.; Li, Y. Numerical and experimental study of water entry problem of two-dimensional wedge. *Ship Sci. Technol.* **2021**, *43*, 53–60.
12. Wang, Y.; Li, M.; Zhang, Z.; Li, S.; Si, G. Numerical simulation on the slamming load in the water-entry process of flatted-bottom body based on the method VOF. *J. Vib. Shock.* **2017**, *36*, 185–189.
13. Du, Y.; Wang, C.; Zhang, N. Numerical simulation on coupled ship motions with nonlinear sloshing. *Ocean. Eng.* **2019**, *178*, 493–500. [CrossRef]
14. Nagi, A.; Yuriy, D.; Roberto, O.; Giles, T.; Walid, A. Experimental investigation of wave-in-deck impact events on a TLP model. *Ocean. Eng.* **2017**, *142*, 541–562.
15. Luo, M.; Rubinato, M.; Wang, X.; Zhao, X. Experimental investigation of freak wave actions on a floating platform and effects of the air gap. *Ocean. Eng.* **2022**, *253*, 111192. [CrossRef]
16. Luo, M.; Koh, C.G.; Lee, W.X.; Lin, P.; Reeve, D.E. Experimental study of freak wave impacts on a tension-leg plat-form. *Mar. Struct.* **2022**, *74*, 102821. [CrossRef]
17. Cuomo, G.; Shimosako, K.; Takahashi, S. Wave-in-deck loads on coastal bridges and the role of air. *Coast. Eng.* **2009**, *56*, 793–809. [CrossRef]
18. Ren, B.; Wang, Y. Experimental study of irregular wave impact on the structurein splash zone spectral analysis. *Ocean. Eng.* **2003**, *30*, 53–60+74. [CrossRef]
19. Zhou, Y.; Chen, G.; Huang, H.; Wang, D. Experimental study on uplift forces of waves on a horizontal plate of an open-wharf. *Ocean. Eng.* **2004**, *19*, 43–50.
20. Paulsen, B.; Sonneville, B.; Meulen, M.; Jacobsen, N. Probability of wave slamming and the magnitude of slamming loads on offshore wind turbine foundations. *Coast. Eng.* **2019**, *143*, 76–95. [CrossRef]

21. Tore, J.; Bernt, J. Numerical and experimental studies of submerged towing of a subsea template. *Ocean. Eng.* **2012**, *42*, 147–154.
22. Issa, R.I. Solution of the implicitly discretised fluid flow equations by operator-splitting. *J. Comput. Phys.* **1986**, *62*, 40–65. [CrossRef]

**Disclaimer/Publisher's Note:** The statements, opinions and data contained in all publications are solely those of the individual author(s) and contributor(s) and not of MDPI and/or the editor(s). MDPI and/or the editor(s) disclaim responsibility for any injury to people or property resulting from any ideas, methods, instructions or products referred to in the content.